Retroreflector Array Transfer Functions

by
David A. Arnold
94 Pierce Road
Watertown, MA 02472-3035
617-924-6812

Contents

Note: This is an abbreviated version of the paper presented at LW13. The complete version can be downloaded from http://nercslr.nmt.ac.uk/sig/signature.html

1. Introduction

The theme of this conference is “Toward Millimeter Accuracy”. There are a number of effects that can cause systematic errors in laser ranging at the millimeter level. These effects are difficult to see in orbital analysis but can be calculated analytically using computer models of the retroreflector array and the laser ranging system.

The data shown in this report has been calculated theoretically. Some of the results are confirmed by experimental data. The rest would required additional experiments to verify whether the analysis is correct.

Some of this work was funded by NASA. The rest was done privately as part of an informal proposal for funding to participate in the activities of the Signal Processing working group. The results of this proposal effort are being presented at this conference to illustrate the kinds of problems that can be studied and the results that can be obtained relative to the goal of achieving millimeter accuracy. The computer models that have been developed are described in Appendix A.

2. Diffraction patterns of single cube corners.

A. Diffraction patterns of a coated circular cube corner.

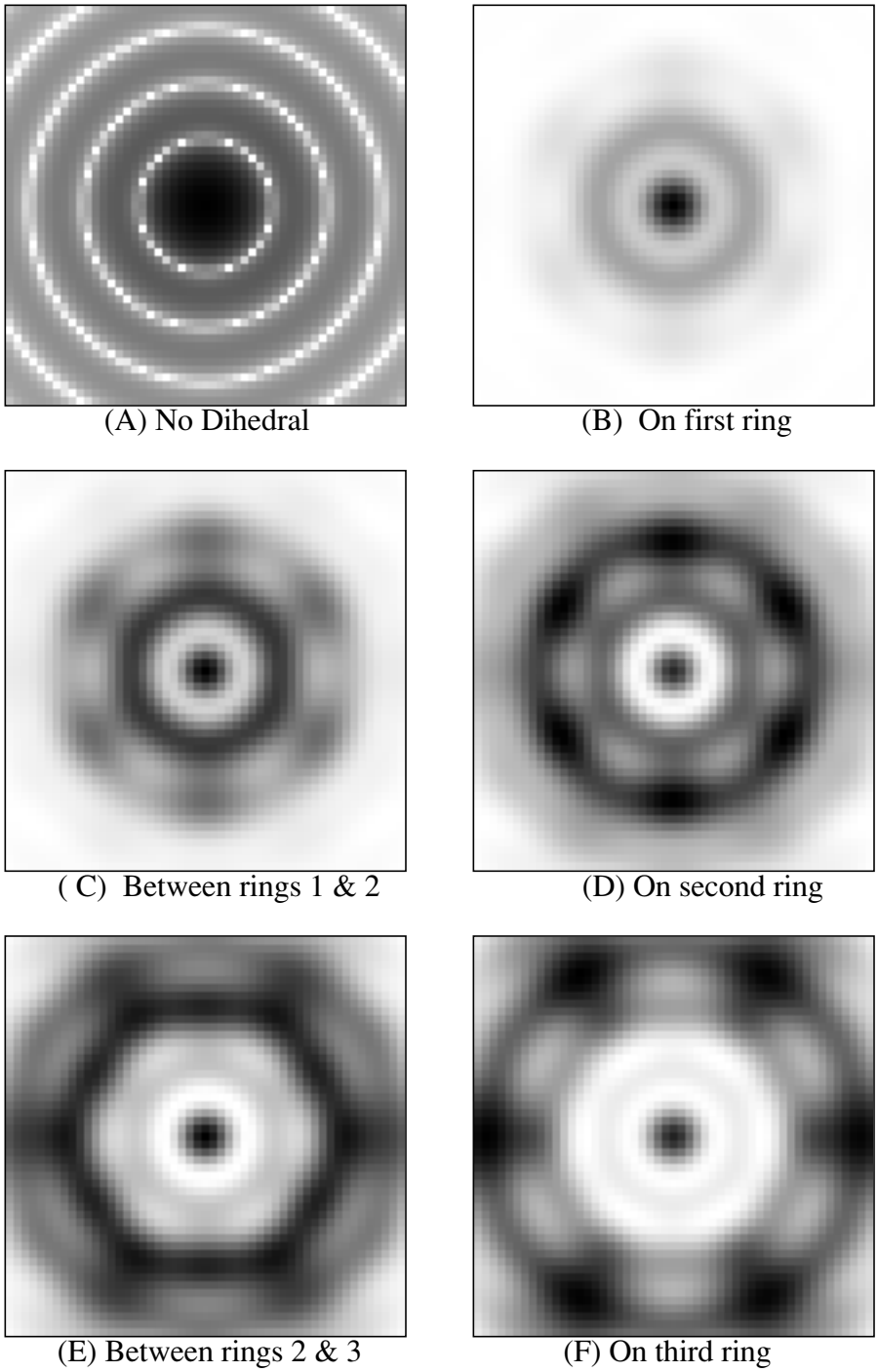

(A) No Dihedral (B) On first ring

(C) Between rings 1 & 2 (D) On second ring

(E) Between rings 2 & 3 (F) On third ring

Figure 1. Coated 1.5 inch cube corner with various dihedral angle offsets.

Figure 1 shows some diffraction patterns of a perfect circular coated 1.5 inch cube corner with index of refraction n =1.461 for different dihedral angle offsets. The size of the plots is from -50 to +50 microradians in both dimensions. The patterns are displayed as inverted gray scale plots. Part (A) is a logarithmic plot. Parts (B) - (F) are linear plots.

The beam spread γ if the three dihedral angles of a cube corner are offset by an angle δ is given by the equation

$$\gamma = \frac{4}{3}\sqrt{6}n\delta \qquad (1)$$

where n is the index of refraction. At normal incidence the geometrical optics solution is six spots in the form of a hexagon.

Part (A) of the figure shows the diffraction pattern with no dihedral angle offset. The diffraction pattern is displayed as a logarithmic plot in order to show the rings. In a linear plot, only the central lobe would be visible. The three rings are at 22.82, 37.40 and 51.63 microradians.

Part (B) shows the diffraction pattern with a dihedral angle offset .986 arc seconds. Using equation (1) for this offset gives a beam spread of 22.82 microradians, the same as the first ring. Because of diffraction effects, the six spots that would exits in the geometrical optics solution coalesce into a smooth ring.

In part (C) the dihedral angle of 1.30 arc seconds is trying to create spots between the first and second rings. The pattern shows hexagonal symmetry outside the first ring.

In part (D) the dihedral angle of 1.62 arc seconds gives a beam spread from equation (1) of 37.40 microradians, the same as the radius of the second diffraction ring. The second ring is the brightest, but is not as smooth as the first ring.

In part (E) the dihedral angle of 1.92 arc sec is trying to put spots between the second and third rings. The pattern is more complicated.

In part (F) the dihedral angle offset of 2.2 arc seconds gives a beam spread from equation (1) of 51.63 arc sec, the same as the third diffraction ring. The third ring is the brightest and there are six spots at the position of the geometrical optics solution.

B. Diffraction patterns of an uncoated circular cube corner.

Figure 2 shows diffraction patterns of a 1.5 inch diameter circular uncoated cube corner. The first column (left) shows the total energy. The second column (middle) shows the component of the reflected energy that is in the same (parallel) polarization state as the input. The third column (right) shows the energy in the orthogonal component. The first column is the sum of columns two and three.

Parts (A), (B), and (C) of figure 2 are for circular polarization with no dihedral angle offset. Part (B) has triangular symmetry and the energy is primarily in the central lobe. Part (C) has hexagonal symmetry and the energy is primarily in the ring of six spots. The total energy in part (A) does not have perfect hexagonal symmetry, but there are six spots around the central lobe that are approximately in the shape of a hexagon.

Circular polarization

No dihedral angle offset

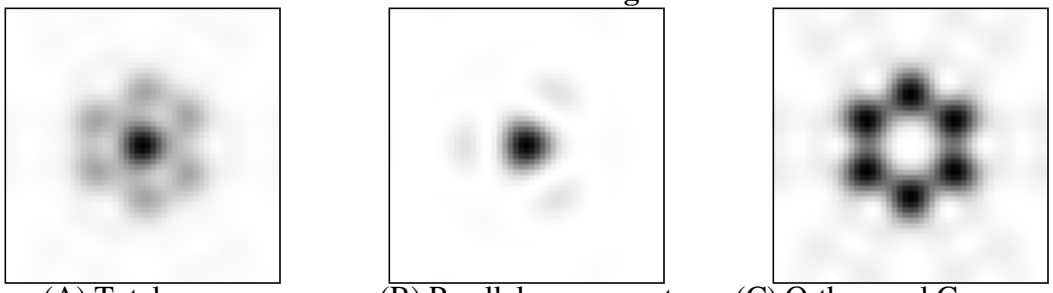

(A) Total energy (B) Parallel component (C) Orthogonal Component

Dihedral angle offset 1.25 arc seconds

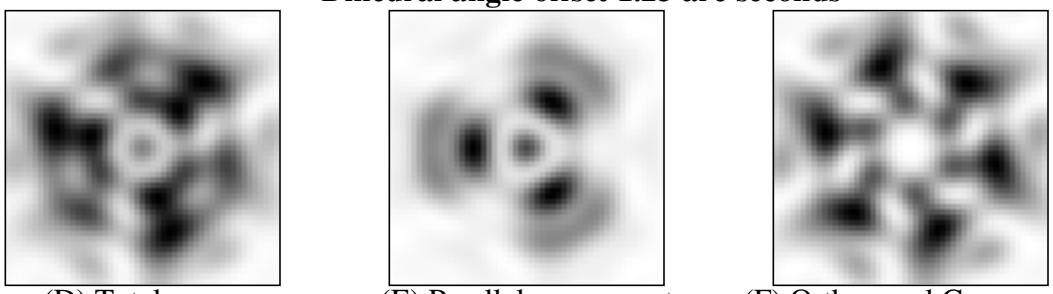

(D) Total energy (E) Parallel component (F) Orthogonal Component

Linear vertical polarization

No dihedral angle offset

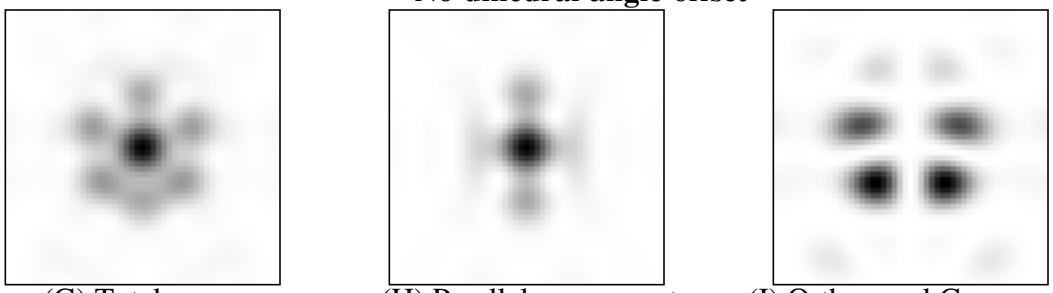

(G) Total energy (H) Parallel component (I) Orthogonal Component

Dihedral angle offset 1.25 arc seconds

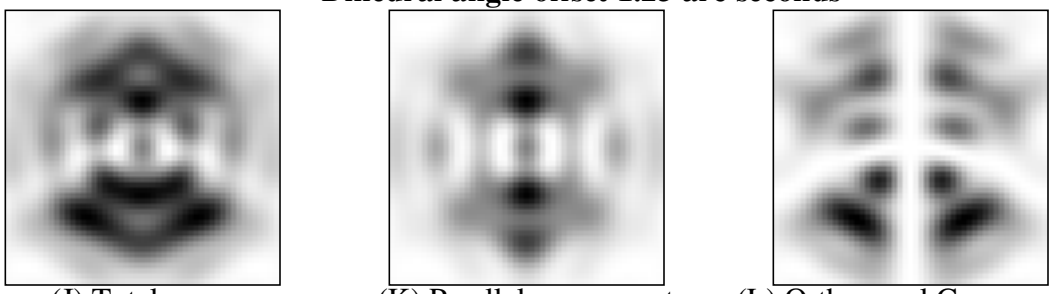

(J) Total energy (K) Parallel component (L) Orthogonal Component

Figure 2. Diffraction pattern of an uncoated 1.5 inch cube corner with, and without, a dihedral angle offset, for circular and linear input polarization.

Parts (D), (E), and (F) are for circular polarization with a dihedral angle offset.

Parts (G), (H), and (I) are with linear vertical polarization and no dihedral angle offset. Parts (H), and (I) show symmetry from left to right. The total energy in part (G) has six spots around the central lobe that are approximately in the shape of a hexagon with left to right symmetry. Parts (G), (H), and (I) have been observed experimentally (see figures 3, 4, and 5 of reference 1).

Parts (J), (K), and (L) are for linear polarization with a dihedral angle offset. There is an interaction between the linear polarization and the dihedral angle offset that creates a "dumbbell" type pattern aligned with the polarization vector. The patterns show left to right symmetry.

With no dihedral angle offset the total energy as shown in parts (A) and (G) has a nearly hexagonal shape. With a dihedral angle offset, the total energy for circular polarization has approximately circular symmetry. The total energy for linear polarization has a "dumbbell" shape.

In an array of cube corners with no dihedral angle offset, the six spots around the central peak can be made into a reasonably smooth ring by having a distribution of orientations for the cube corners. However, this cannot be done with a dihedral angle offset and linear polarization because the interaction between the polarization and the dihedral angle offset produces a "dumbbell" shaped pattern aligned with the polarization vector.

3. Basic principles of retroreflector array design.

A. Geometry of the array.

For a single cube corner, the range correction can be calculated to a high degree of accuracy from the index of refraction and the angle of incidence. However, a single cube may not provide adequate signal strength or adequate angular coverage.

For a planar array of identical cubes all at the same orientation, the range correction will be the same as that of a single cube at the center of mass of the array. In practice, manufacturing imperfections cause variations in the reflecting properties of different cubes that can cause changes in the range correction.

The diffraction pattern of a cube corner depends on the incidence angle. For an array of cubes at different orientations (such as a spherical array), the range correction will be different at each point in the far field diffraction pattern.

B. Size of the array

A single retroreflector acts like a point reflector. There is no pulse spreading and no uncertainty in the range correction. If the target consists of a number of cube corners at different distances along the line of sight, there will be spreading of the pulse. In order to minimize range uncertainties, the range depth of the array should be kept as small as possible.

C. Velocity aberration and diffraction.

Because of velocity aberration, the center of the return beam is deflected away from the source by the angle $2v/c$ where v is the component of the satellite's velocity perpendicular to the line of sight. The signal at the receiver will depend on the intensity of the diffraction pattern of the cube corners at an angle $2v/c$ from the center of the return beam. Having a smooth diffraction pattern at $2v/c$ will minimize the variations in the cross section and range correction.

The smoothest part of the diffraction pattern is the central lobe. For a coated cube corner the first zero is at $1.22 \lambda/D$ where λ is the wavelength and D is the diameter of the cube corner. In low earth orbit, the cube corner would have to be quite small to put the receiver on the central lobe. Using the first ring as in Figure 1(B) would also produce a smooth pattern with a coated cube corner and allow the use of a larger cube.

Uncoated cubes have a natural beam spread with six spots around the central lobe. This is the result of polarization effects caused by total internal reflection at the back faces. The beam is wider than for a coated cube without the need for a dihedral angle offset.

D. Thermal gradients

The diffraction pattern of a cube corner can be severely degraded by thermal gradients in the material. The larger the cube corner the greater the sensitivity to thermal gradients because of the longer optical path lengths and the larger total temperature difference for a particular gradient. With a linear vertical temperature gradient the effect on the central irradiance of a coated cube corner is proportional to the square of the diameter of the cube corner. Another problem in coated cube corners is absorption of sunlight at the metalized back reflecting faces.

E. Dihedral angle offsets.

It is difficult (and expensive) to manufacture a cube corner with a specific dihedral angle offset. The smaller the tolerance the greater the cost. A tolerance less than .5 arc seconds could result in a lot of cube corners being rejected or re-manufactured.

One reason for having a specific dihedral angle offset is to be able to model the transfer function of the array. For the purposes of modeling it does not really matter what the dihedral angle is as long as its value is known. Measuring and recording the angles can be more cost effective than setting tight tolerances as long at the angles are within the range needed to achieve the necessary beam spread.

F. Coated vs uncoated cube corners.

The choice of coated or uncoated cubes will depend on the requirements. Some of the properties to be considered are the following:

a. Uncoated cube corners lose total internal reflection starting at about 17 degrees incidence angle. In a spherical satellite this has the effect of reducing the range depth. Having less range depth reduces the pulse spreading, coherent variations, and possible variations in range correction.

b. The reflection from an uncoated cube corner has energy in both polarization components regardless of the input polarization. Coherent interference occurs only within each polarization component. In other words, the x component cannot interfere with the y component and vice versa. This results in better averaging of coherent interference by a factor of $\sqrt{2}$.

c. Uncoated cubes have a higher reflectivity at normal incidence than coated cubes because of total internal reflection. The helps to compensate for the loss of signal past the cutoff angle for total internal reflection so as to produce a stronger signal with less range depth.

d. Uncoated cubes have no back faces to absorb solar radiation and contribute to thermal gradients.

e. Uncoated cubes have no back faces that could peel or be subject to deterioration over long periods of time.

f. The natural beam spread in an uncoated cube can eliminate the need for a dihedral angle offset. There is a cost advantage to specifying the dihedral angle as 90 degrees with some tolerance. A negative dihedral angle offset produces about the same pattern as a positive dihedral angle offset. Specifying the dihedral angle as 90 degrees with a tolerance of 1/2 arc second gives the same consistency of performance as specifying the angle as 90 degrees plus 1/4 arc second with a tolerance of 1/4 arc second.

g. The cutoff angle in an uncoated cube corner can vary from about 17 degrees to the normal cutoff of about 57 degrees depending on the orientation of the cube corner. To avoid anomalies in the transfer function for a spherical satellite it is necessary to have a distribution of orientations of the cube corners. A distribution of orientations is also desirable to smooth out the pattern since there are six spots outside the central lobe.

h. If linear polarization is used the transfer function with uncoated cubes has a "dumbbell" shape which can introduce a systematic error if no correction is applied. The problem can be corrected by applying a correction for the asymmetry. The asymmetry can be eliminated by using circular polarization.

4. Transfer function of the Lageos retroreflector array.

A. Cross section and range correction at a single orientation

(see original version)

B. Average cross section and range correction

(see original version)

C. Spinning satellite.

Both Lageos 1 and Lageos 2 were launched spinning. The spin rate decreases with time and is currently quite low for Lageos 1. Even if the satellite were not spinning, the viewing angle would vary throughout a pass as a result of the observing geometry.

Figure 6 shows the range correction for linear polarization at two points in the far field with the satellite spinning about its symmetry axis. The first point is on the vertical velocity aberration axis at x = 0, y = 35 microradians. The red curve is the centroid and the green curve is the half-max range correction. The second point is on the horizontal velocity aberration axis at x = 35, y = 0 microradians. The purple curve is the centroid and the blue curve is the half-max range correction. The range correction is always greater on the vertical axis. The average value of each range correction in millimeters is shown below.

Case	Average	rms	color
Centroid (0,35)	243.3	1.5	red
Centroid (35,0)	240.2	1.7	purple
Halfmax (0,35)	250.6	0.6	green
Halfmax (35,0)	249.9	0.7	blue
Centroid (both)	241.7	2.2	
Halfmax (both)	250.2	0.7	

The difference between the average centroid at the two points in the far field is 3.1 millimeters. The difference between the average half-max range corrections at the two points is .7 millimeters.

Figure 7 plots the difference between the range corrections at the two points in the far field. The red curve is for the centroid and the green curve is for half-max.

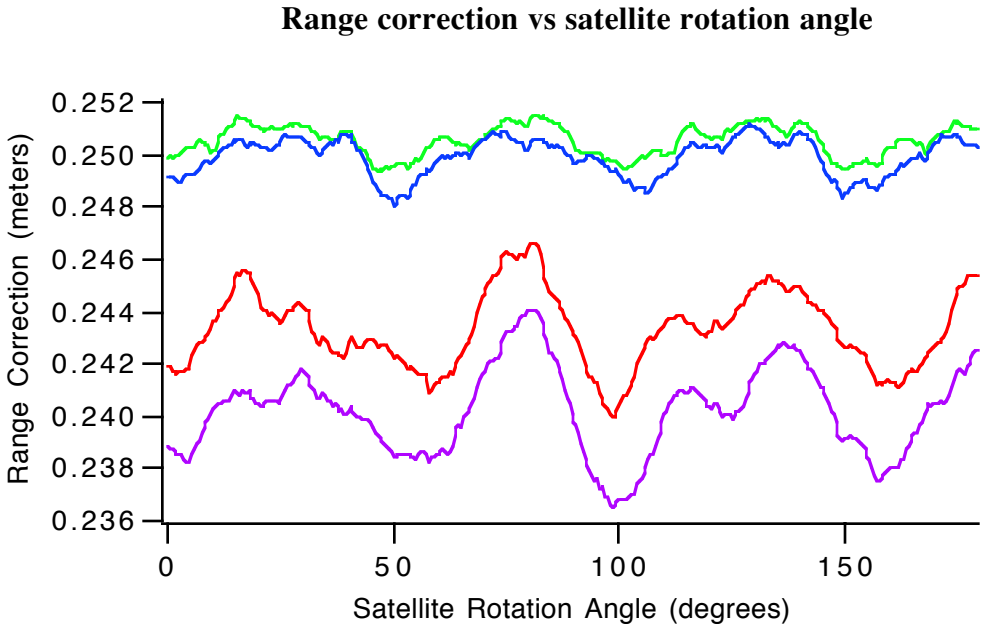

Figure 6. Centroid and half-max range correction vs satellite rotation angle at velocity aberration (0,35) and (35,0) μrad with linear vertical polarization (y-axis).
A. Velocity aberration x = 0 μrad, y = 35 μrad.
red = Centroid
green = Half-max
B. Velocity aberration x = 35 μrad, y = 0 μrad
Purple = Centroid
Blue = Half-max

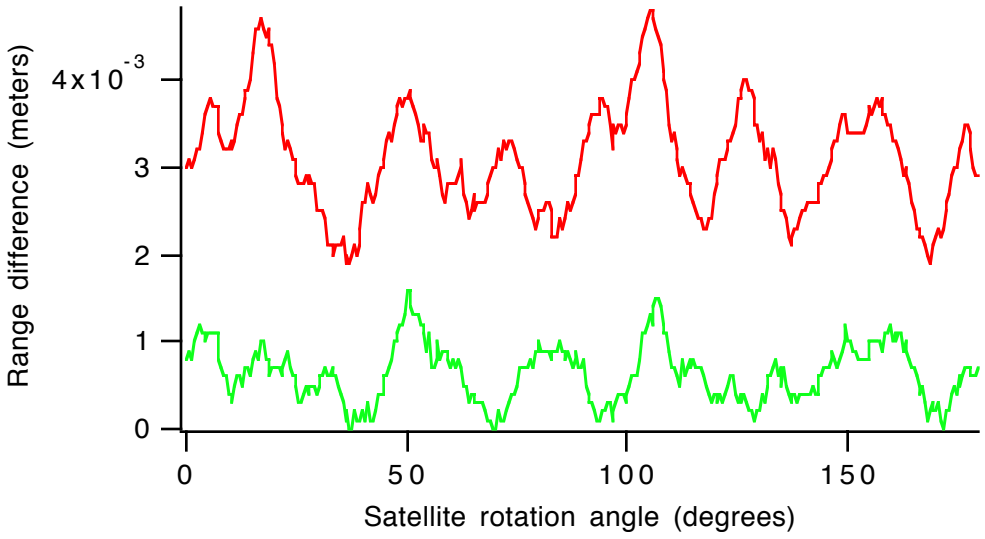

Figure 7. Range correction at (0,35) minus range correction at (35,0) μrad.
Red = centroid(0,35) - centroid(35,0)
Green = half-max(0,35) - half-max(35,0)

The variations in the half-max range correction are smaller than for the centroid since the half-max correction tends to measure the leading edge of the pulse. These calculations are for the incoherent case. They do not include the effects of coherence or photon quantization. These effects cause fluctuations in the range correction from pulse to pulse and can introduce a bias in multi-photoelectron measurements depending on the type of detection algorithm used.

D. Coherent variations of the range correction

(see original version)

E. Signal strength dependence.

The signal processed by a laser receiving systems consists of a discrete number of photoelectrons. If the number of photoelectrons is large, the signal should be a good representation of the received signal. If the signal consists of a small number of photoelectrons, there will be variations in the shape of the pulse due to photon quantization.

For half-max detection systems, there will be a shift in the range correction as a function of signal strength. For single photoelectron returns, the average position of the photoelectron will be at the centroid of the retroreflector array. For half-max systems with a strong signal, the average measured position will be the half-max point on the leading edge of the pulse.

Figure 8 shows the results of a Lageos simulation with different pulse detection algorithms for average signal strengths from .1 to 1000 photoelectrons. The simulation is done for an orientation of the satellite where the centroid is 241 millimeters from the center of the array.

The rise time of the photo-multiplier is assumed to be .125 nanosecond and the half-max, half-width of a single photoelectron is 8.6 millimeters. For a photoelectron at the centroid the half-max point of the return is at 241 + 8.6 = 249.6 millimeters.

The transmitted pulse used in the simulation is 200 picoseconds which gives a one-way half-max, half width of 15 millimeters for the transmitted pulse. The half width of the return from the Lageos array (with a zero length input pulse) is about 21 millimeters. Convolving the transmitted pulse with the Lageos array and the photo-multiplier response gives a half width of about 27 millimeters for the return pulse. Adding this to the centroid of 241 millimeters gives a value of 268 millimeters for the half-max point on the return pulse for the strong signal case.

The top curve in blue in figure 8 is the average position of the half-max point on the return pulse vs signal strength. It starts out at 250 millimeters for single photoelectron returns and rises to 268 millimeters for strong signals. The green curve is the half-area point and the red curve (partially obscured by the green curve) is the centroid.

Figure 9 shows the variation of the range correction with signal strength for a set of target measurements. For the target measurements there is no spreading due to the target. The only spreading is due to the width of the transmitted pulse and the spreading of the photo-multiplier. This give a combined spreading of about 17 millimeters. Adding this to the centroid of 241 millimeters gives a half-max point of 258 millimeters for the strong signal case.

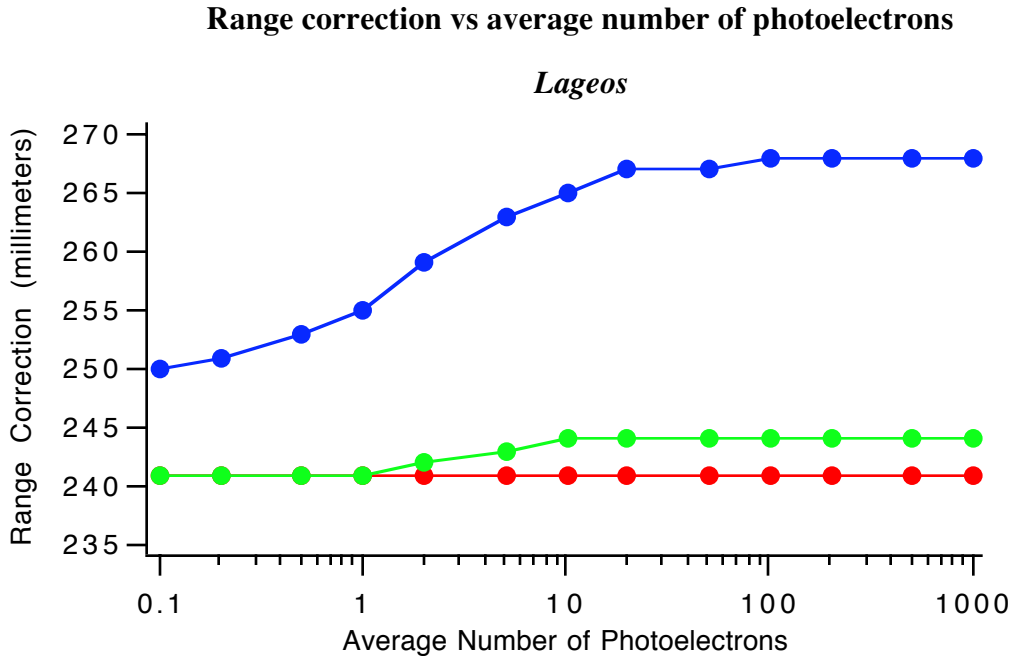

Figure 8. Range correction for Lageos vs number of photoelectrons.
Blue = Half-Max
Green = Half Area
Red = Centroid

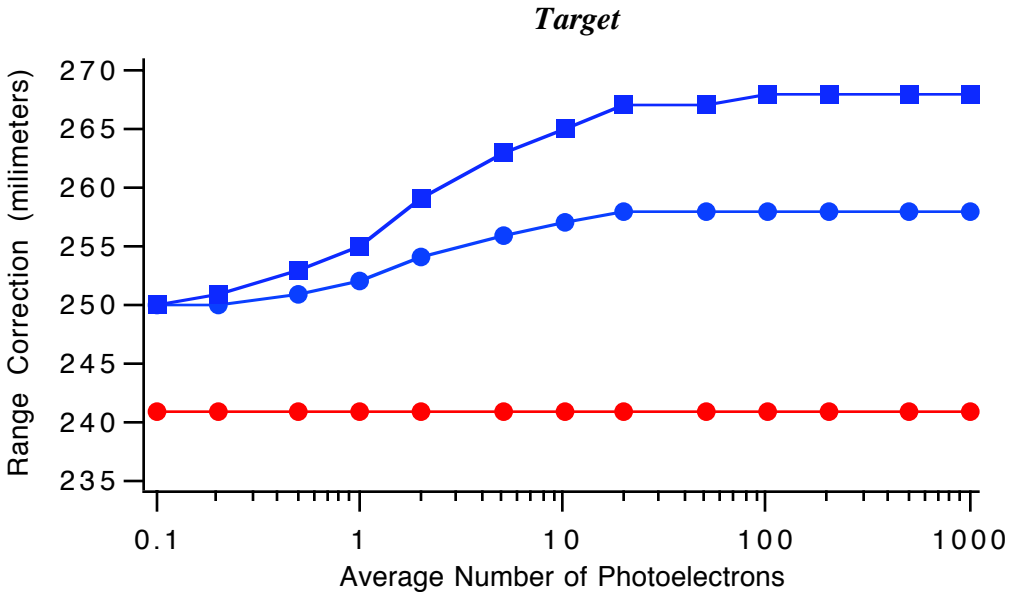

Figure 9. Range correction for target calibration compared to Lageos Half-Max
Blue = Half-Max
Square = Lageos
Circle = Target
Red = Centroid and Half Area

The blue curve with circles in figure 9 is the position of the half-max point for the target measurements vs signal strength. The curve with blue squares is the half-max position for Lageos for comparison. The difference between the blue squares and the blue circles is the range correction that would need to be applied to Lageos range measurements as a function of signal strength. It is about 10 millimeters for this set of station parameters.

5. Transfer function of the TOPEX retroreflector array.
(see original version)

6. Transfer function of the WESTPAC retroreflector array
(see original version)

References

1. OPTICAL PROPERTIES OF THE APOLLO LASER RANGING RETROREFLECTOR ARRAYS, R.F Chang, C.O. Alley, D.G. Currie, and J.E. Faller, Space Research XII, Akademie-Verlag, Berlin, 1972.

2. OPTICAL AND INFRARED TRANSFER FUNCTION OF THE LAGEOS RETROREFLECTOR ARRAY, Grant NGR 09-015-002, David A. Arnold, May, 1978.

3. METHOD OF CALCULATING RETROREFLECTOR-ARRAY TRANSFER FUNCTIONS, David A. Arnold, Smithsonian Astrophysical Observatory SPECIAL REPORT 382.

4. Prelauch Optical Characterization of the Laser Geodynamic Satellite (LAGEOS 2), Peter O. Minott, Thomas W. Zagwodzki, Thomas Varghese, and Michael Selden.

Acknowledgments

The author wishes to express his appreciation to Vladimir Vasiliev for providing specifications of the WESTPAC retroreflector array, Michael Selden for providing information on the prelaunch tests of Lageos 2, and Reinhart Neubert for many helpful discussions. The analyses in sections 4.A and 4.D for Lageos, and section 5 for Topex, and the development of the original versions of the programs listed in Appendix A were supported by NASA funding.

Appendix A. Description of analysis programs

The original versions of these programs were written in the early 70's. The current versions have a number of new features that have been added recently.

TRANSFR This program is described in SAO Special Report 382. It is optimized for computing an N x N diffraction pattern of an array. Matrices for cross section, centroid range correction, and pulse spread (r.m.s width) are computed. The program has been recently updated to include recessed cube corners such as used on WESTPAC.

RETURN This program is like TRANSFR except that it uses versions of the diffraction subroutines that compute only a single point in the far field. The pulse shape is computed to determine the centroid, half-area, peak, and half-max points. The program can also model coherent interference and photon quantization using a random number generator. The program has been recently recreated after not being used for 25 years. Some work remains to be done to get the program fully operational.

LRSS (Laser Receiving System Simulation). This program can use a pulse shape computed by RETURN or generate a Gaussian input pulse. The average number of photoelectrons is used to generate random signal strengths using a Poisson distribution. Photoelectrons are randomly distributed in the area under the pulse. The pulse shape is plotted and analyzed for various detection algorithms - centroid, half-area, half-max, and pulse analyzer (with a centroid algorithm). The program was recently recreated after not being used for 25 years.

DIFRACT This program computes the diffraction program of a single cube corner at normal incidence by numerical integration of a 101 x 101 array of phases. It can model the effect of a temperature gradient expressed as a quadratic function in three dimensions with origin at the center of the front face. New features have been added to model various types of curvature of the wavefront expressed as a polynomial function of the position from the center of the front face. Modification have been added to produce phase plots, and simulated interferograms.

ECCENTRIC This program computes signal strength in photoelectrons for a specific set of station parameters for a satellite in an eccentric orbit. It is a recently written program based on an old program, RNGEQN, which modeled only circular orbits. The cross section of the satellite can be given as a constant, a table vs velocity aberration, or a two-dimensional matrix. The program can accept a set of matrices vs incidence angle on the array assuming the satellite is gravity gradient stabilized. The cross section matrices are computed by program TRANSFR

Appendix B. Tables for signal strength dependence of the Lageos range correction. (see original version)

Appendix C. Theory of programs RETURN and LRSS (see original version)